Three-dimensional numerical inversion of pneumatic cross-hole tests in unsaturated fractured tuff
1. Methodology and borehole effects

Velimir V. Vesselinov,[1] Shlomo P. Neuman, and Walter A. Illman[2]

Department of Hydrology and Water Resources, University of Arizona, Tucson, Arizona, USA

Abstract. We describe a three-dimensional numerical inverse model for the interpretation of cross-hole pneumatic tests in unsaturated fractured tuffs at the Apache Leap Research Site (ALRS) near Superior, Arizona. The model combines a finite volume flow simulator, FEHM, an automatic mesh generator, X3D, a parallelized version of an automatic parameter estimator, PEST, and a geostatistical package, GSTAT. The tests are simulated by considering single-phase airflow through a porous continuum, which represents primarily interconnected fractures at the site. The simulator solves the airflow equations in their original nonlinear form and accounts directly for the ability of all packed-off borehole intervals to store and conduct air through the system. Computations are performed in parallel on a supercomputer using 32 processors. We analyze pneumatic cross-hole test data, previously conducted by our group at ALRS, in two ways: (1) by considering pressure records from individual borehole monitoring intervals one at a time, while treating the rock as being spatially uniform, and (2) by considering pressure records from multiple tests and borehole monitoring intervals simultaneously, while treating the rock as being randomly heterogeneous. The first approach yields a series of equivalent air permeabilities and air-filled porosities for the rock volume being tested, having length scales of the order of meters to tens of meters. The second approach yields a high-resolution geostatistical estimate of how air permeability and air-filled porosity, defined on grid blocks having a length scale of 1 m, vary spatially throughout the tested rock volume. It amounts to three-dimensional pneumatic "tomography" or stochastic imaging of the rock, a concept originally proposed by one of us in 1987. The first paper of this two-part series describes the field data, the model, and the effect of boreholes on pressure propagation through the rock. The second paper implements our approach on selected cross-hole test data from ALRS.

1. Introduction

A total of 44 cross-hole air injection tests have been conducted by *Illman et al.* [1998] [see also *Illman*, 1999] in 16 vertical and inclined boreholes drilled into unsaturated fractured tuff at the Apache Leap Research Site (ALRS) near Superior, Arizona. Their purpose was to characterize the bulk pneumatic properties and connectivity of fractures at the site on scales ranging from meters to several tens of meters. The design, conduct, and type curve interpretation of one of these tests have recently been described by *Illman and Neuman* [2001]. The type curves they used have been modified after *Hsieh and Neuman* [1985] to consider single-phase airflow and extended to consider the effects of storage and skin in monitoring intervals. Cross-hole type curves of pressure derivatives and recovery were included for improved pneumatic characterization of the site.

Illman and Neuman [2001] analyzed recorded pressures in each monitoring interval separately from those in other intervals, while treating the fractured rock as a uniform, isotropic porous continuum. Each record yielded an equivalent directional air permeability and air-filled porosity for fractures that connect the corresponding monitoring and injection intervals, representing rock volumes with length scales ranging from meters to a few tens of meters. Both parameters were found to vary considerably from one monitoring interval to another, reflecting the nonuniform nature of pneumatic rock properties at ALRS. The geometric mean of these equivalent permeabilities exceeded by a factor of 50 that obtained earlier by *Guzman et al.* [1996] from single-hole pneumatic injection tests, on a nominal scale of 1–3 m [*Vesselinov*, 2000] (single-hole tests yield only limited information about porosities, which therefore cannot be meaningfully compared with cross-hole results). On the basis of these and related studies conducted at the site by various University of Arizona researchers, *Illman and Neuman* [2001] concluded that the pneumatic pressure behavior of unsaturated fractured tuffs at ALRS can be described quite accurately by means of linearized single-phase airflow equations; this behavior can be interpreted by treating the rock as a continuum on scales ranging from meters to tens of meters; the continuum is representative primarily of interconnected fractures; as these fractures are filled primarily with air, their pneumatic permeabilities and porosities are close to the bulk intrinsic properties of fractures at the site; these intrinsic prop-

---

[1]Now at Hydrology, Geochemistry, and Geology Group, Los Alamos National Laboratory, Los Alamos, New Mexico, USA.
[2]Now at Department of Geosciences, University of Iowa, Iowa City, Iowa, USA.

erties vary randomly with location and direction across ALRS; and permeability depends strongly on the scale at which it is determined.

Type curve methods provide a relatively simple, fast and reliable way to interpret the results of pressure interference tests between boreholes in porous and fractured geologic media. Because type curves are usually based on analytical solutions of the corresponding flow equations, they typically treat the medium as being composed of one, or very few, uniform constituents such as aquifers, aquitards, faults, dikes, and/or fractures. For this reason, they yield equivalent properties of the medium (permeability, specific storage, or porosity) on scales comparable to distances between an injection or pumping well that generates a pressure signal and monitoring wells in which pressure responses to this signal are observed. Type curve methods cannot provide detailed information about the spatial variability of medium properties on scales smaller than these distances. To obtain such information, *Neuman* [1987] suggested that the rock be treated as a stochastic continuum and its properties be estimated by the simultaneous numerical inversion of multiple pressure signals, sent across the rock from various boreholes in various directions. Neuman's suggestion arose in the context of hydraulic cross-hole tests conducted by *Hsieh et al.* [1985] in a saturated crystalline rock mass near Oracle, Arizona, which, however, have not been interpreted in this way. Since the idea is akin to geophysical characterization methods, such as seismic and electromagnetic tomography, Neuman termed his proposed approach "hydraulic tomography."

More recently, the concept of hydraulic tomography has been explored by *Bohling* [1993], *Tosaka et al.* [1993], *Gottlieb and Dietrich* [1995] [see also *Gottlieb*, 1992], *Masumoto et al.* [1995, 1996, 1998], *Butler et al.* [1999], and *Yeh and Liu* [2000]. *Tosaka et al.* [1993] used an inverse model to analyze simultaneously a series of transient cross-hole tests in two- and three-dimensional synthetic media. They treated porosity as a known constant and allowed permeability to vary from one grid block to another across each flow domain. Whereas they were able to reproduce quite accurately the spatial pattern of synthetic permeabilities, they were less successful in reproducing their magnitudes. The same was true about a study by *Gottlieb and Dietrich* [1995] of transient flow between a doublet of wells in a synthetic two-dimensional aquifer. *Masumoto et al.* [1998] extended the analysis of *Tosaka et al.* [1993] to synthetic multirate injection and recovery tests. *Butler et al.* [1999] discussed the application of data collected from multilevel sampling wells to obtain tomographic characterization of rock properties. Most recently, *Yeh and Liu* [2000] developed a sequential geostatistical method to estimate the hydraulic conductivity distribution of a hypothetical, two-dimensional aquifer (assuming that the spatial covariance of the permeabilities is known).

Huang et al. [1999] interpreted simultaneously a series of pneumatic cross-hole tests at Yucca Mountain by treating porosity as a known constant, dividing the flow domain into a number of zones having uniform pneumatic properties, and estimating the permeabilities of these zones through manual calibration by trial and error. *Martinez-Landa et al.* [2000] used an inverse model to estimate the uniform permeabilities of major fractures and the surrounding matrix by analyzing simultaneously the results of five hydraulic interference tests, conducted as part of the Full Engineered Barrier Experiment (FEBEX) at the Grimsel site in Switzerland. *Sauer et al.* [1999] interpreted simultaneously a series of pumping tests in a sys-

tem of aquifers and aquitards having uniform anisotropic properties. *Karasaki et al.* [2000] used a "binary inversion method" developed by *Cook* [1996] to identify high-permeability fracture connections between boreholes in granite at a field site in California based on multiple cross-hole injection tests. They considered it infeasible to estimate the hydraulic properties of the rock based on these tests.

In this paper we describe a three-dimensional numerical inverse model for the interpretation of cross-hole pneumatic tests conducted by *Illman et al.* [1998] in unsaturated fractured tuffs at ALRS. The model simulates single-phase airflow through a porous continuum which on the basis of findings by *Guzman et al.* [1994, 1996] and *Guzman and Neuman* [1996] (later summarized by *Chen et al.* [2000] and *Illman and Neuman* [2000, 2001]), we take to represent primarily interconnected fractures at the site. The simulator solves the airflow equations in their original nonlinear form and accounts directly for the ability of all packed-off borehole intervals to store and conduct air through the system.

We analyze the pneumatic cross-hole test data in two ways: (1) by considering pressure records from individual borehole monitoring intervals one at a time, while treating the rock as being spatially uniform, and (2) by considering pressure records from multiple tests and borehole monitoring intervals simultaneously, while treating the rock as being randomly heterogeneous. The first approach yields a series of equivalent air permeabilities and air-filled porosities for rock volumes having length scales ranging from meters to tens of meters, represented nominally by the distances between corresponding injection and monitoring intervals. The second approach yields a high-resolution geostatistical estimate of how air permeability and air-filled porosity, defined on grid blocks having a length scale of 1 m, vary spatially throughout the tested rock volume. It amounts to three-dimensional pneumatic "tomography" or stochastic imaging of the rock, as proposed by *Neuman* [1987]. The first paper of this two-part series describes the field data, the model, and the effect of boreholes on pressure propagation through the rock. The second paper [*Vesselinov et al.*, this issue] (hereinafter referred to as paper 2) implements our inverse methodology on selected cross-hole test data from ALRS.

2. Cross-Hole Tests at ALRS

2.1. Site and Test Description

For a description of ALRS and cross-hole pneumatic injection tests conducted at the site the reader is referred to *Illman et al.* [1998], *Illman* [1999], *Illman and Neuman* [2001], and *Vesselinov* [2000]. Here we only mention that the test site includes 22 vertical and inclined (at 45°) boreholes, which have been completed to a maximum depth of 30 m within a layer of partially welded unsaturated tuff. The upper 1.8 m of each borehole is cased. Cross-hole testing was conducted in borehole sets V, W, X, Y, and Z that span a volume of rock on the order of 60,000 m³ (Figure 1). A surface area of ~1200 m² was covered with a thick plastic sheet to minimize infiltration and evaporation before and during the tests. A pneumatic cross-hole test consisted of injecting air at a constant mass flow rate into a relatively short packed-off interval in one borehole and monitoring air pressure in various packed-off intervals in this and 15 other boreholes. At the injection point, pressure was measured in situ within the packed-off interval, not in the injection line at the ground surface. Therefore pressure losses
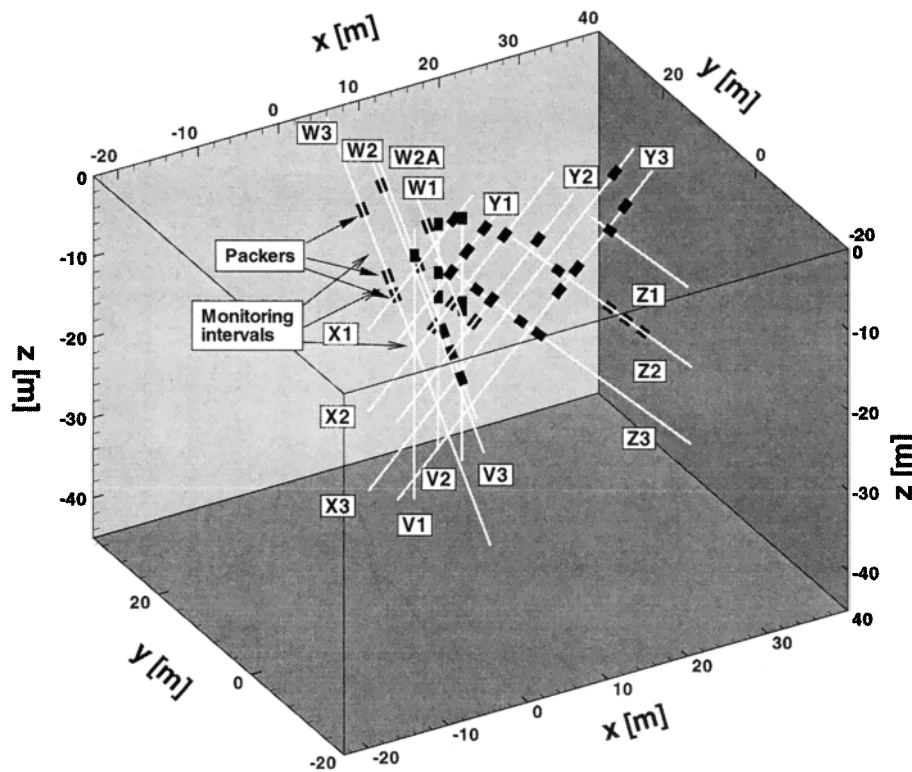
Figure 1. Location of packers in boreholes during cross-hole tests PP4-7 at ALRS.

within the injection line should not play any role in our analysis. During each test, temperature was recorded in each borehole interval together with relative barometric pressure, air temperature, and relative humidity at ground surface.

We perform numerical inverse analyses on 5 of the 44 cross-hole tests conducted at the site. These so-called point-to-point tests are labeled PP4, PP5, PP6, PP7, and PP8 (Table 1). Tests PP4, PP5, PP6, and PP7 were conducted with the packer configuration depicted in Figure 1. In test PP8 the packers in X3 and Y3 were positioned 5.5 and 5.0 m, respectively, lower along the borehole axes than is indicated in Figure 1. The 16 test boreholes contained 38 packed-off intervals that varied in length from 0.5 to 42.6 m. When a single packer is used to isolate a borehole segment, the corresponding interval is named after the borehole (e.g., X1). Multiple intervals are numbered sequentially from top to bottom (e.g., X2-1, X2-2, X2-3). As boreholes V2 and W2 are interconnected, the intervals V2-3 and W2 are linked, and so the actual number of intervals was 37. Pressure data from this and four other intervals (Y1-1, Y1-3, V2-1, W3-3) were found to be unreliable, further reducing the number of working intervals to 32.

During tests PP4 and PP8, air was injected at a constant mass rate of 1×10^{-3} kg/s (50 L/min at standard conditions of $T = 20°C$ and $p = 101$ kPa) into the middle interval of borehole Y2. During tests PP5, PP6, and PP7, air was injected into the middle intervals of boreholes X2, Z3, and W3, respectively. Injection during these three tests was conducted first at one constant rate, and later at a higher rate. We process only data from the first step, conducted at a mass injection rate of 1×10^{-4} kg/s (5 L/min). The injection intervals measured 1 m (PP7) and 2 m (PP4, PP5, PP6, and PP8) in length (Table 1). Distances between injection and observation intervals ranged from 1 to 30 m.

Discrete pressure data recorded in the various test intervals during tests PP4, PP5, and PP6 are shown by small solid dots on log-log plots in Figures 2, 3, and 4, respectively. Similar plots for tests PP7 and PP8 can be found in the work by *Vesselinov* [2000]. The data represent change in absolute air pressure with time relative to pressure at the start of a test. Pressure measurements were taken every 10 s during each test. Figures 2–4 show noise in the pressure data due to barometric pressure fluctuations or other extraneous phenomena. For purposes of inverse analysis we filtered out this noise, as explained in paper 2.

Table 1. Point-to-Point Cross-Hole Tests Interpreted by Numerical Inverse Model

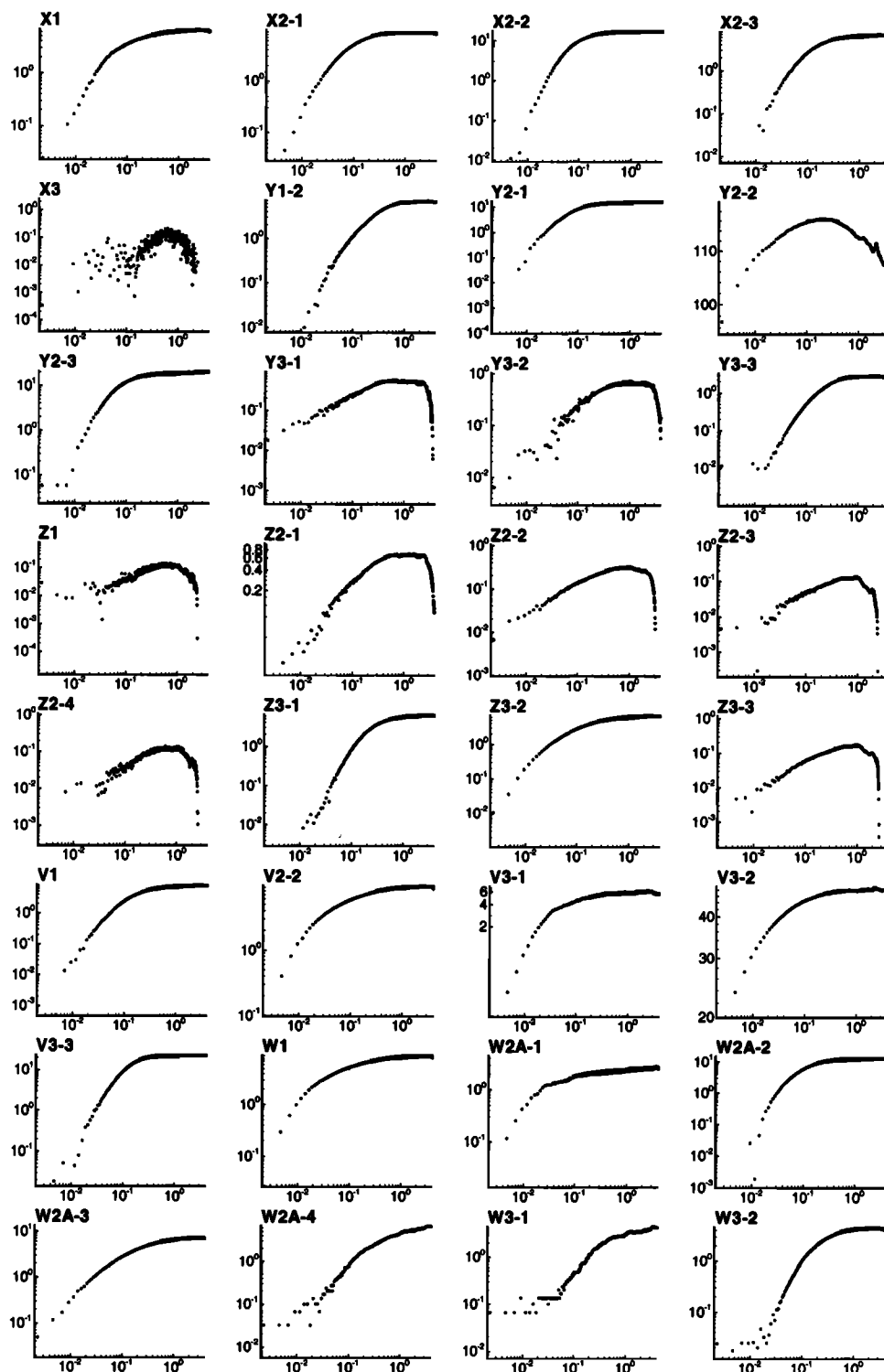| Cross-Hole Test	Injection Interval	Length, m	Duration, days	Injection Rate, L/min	Injection Rate, kg/s
PP4	Y2-2	2.0	3.95	50.0	1.0×10^{-3}
PP5	X2-2	2.0	1.95	5.0	0.1×10^{-3}
PP6	Z3-2	2.0	1.70	5.0	0.1×10^{-3}
PP7	W3-2	1.0	1.90	5.0	0.1×10^{-3}
PP8	Y2-2	2.0	0.84	50.0	1.0×10^{-3}

Figure 2. Log-log plots of observed pressure buildup (kPa) versus time (days) during test PP4.

2.2. Barometric Pressure Effects

Barometric pressure varied significantly during test PP4, having dropped by more than 1 kPa (Figure 5). This has visibly affected late time air pressures recorded in intervals X3, Y3-1, Y3-2, Z1, Z2-1, Z2-2, Z2-3, Z2-4, and Z3-3 (Figure 2). The relationship between air pressure in four of these intervals and

barometric pressure is illustrated in Figure 5. It appears that barometric pressure fluctuations affect the deepest interval (Z3-3) in borehole Z3 more than they affect the upper two intervals (Z3-1 and Z3). This observation is consistent with the single-hole tests conducted in the same borehole [*Rasmussen et al.*, 1990] which reveal the presence of a highly permeable zone
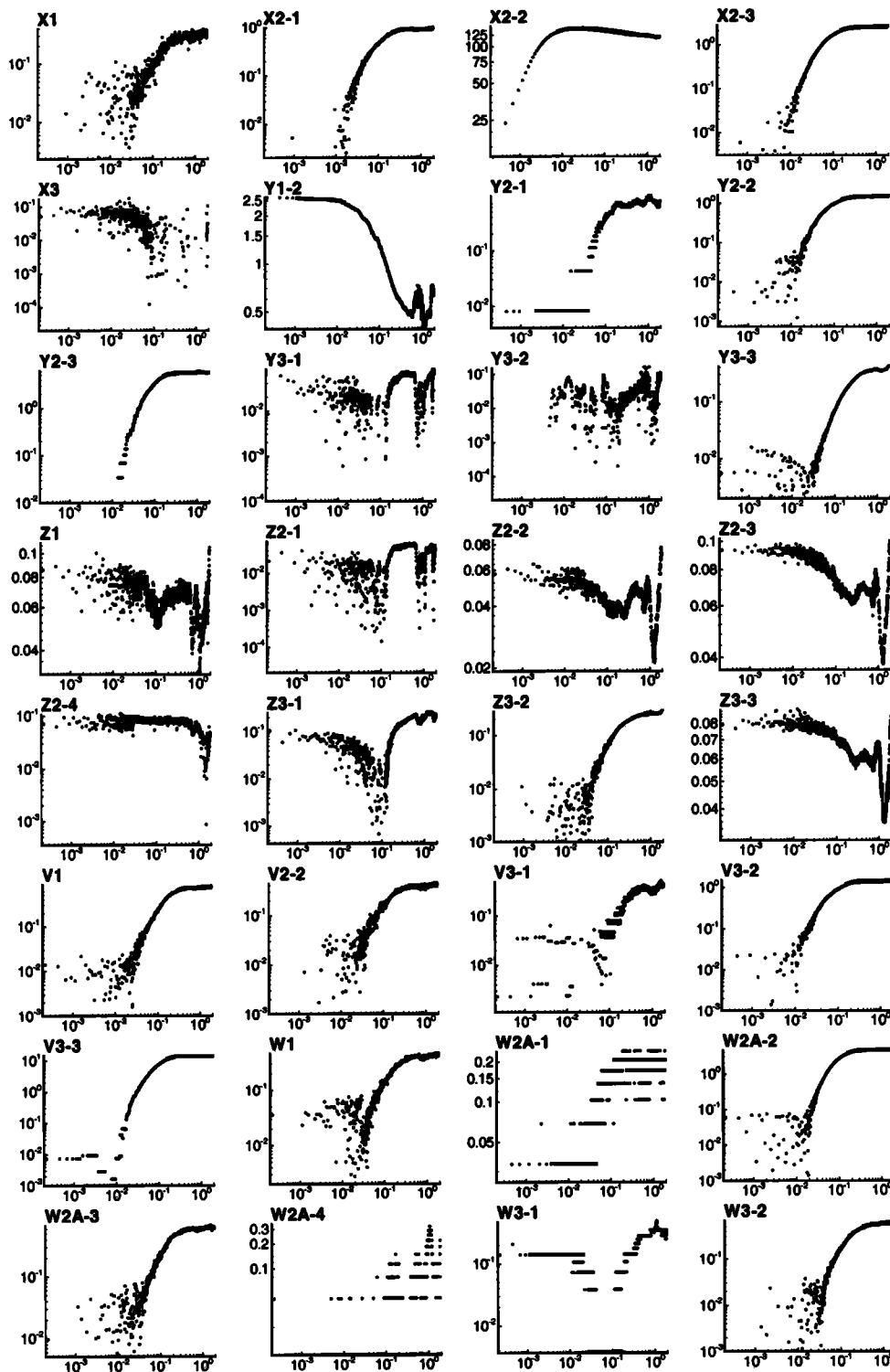
Figure 3. Log-log plots of observed pressure buildup (kPa) versus time (days) during test PP5.

around interval Z3-3. The Z boreholes are located close to a cliff face, and this permeable zone is most probably connected to the atmosphere.

In our inverse analysis we ignore data that are markedly affected by barometric pressure. Though our model can account for known variations in barometric pressure at the sur-

face, we prefer not to do so because our barometric pressure data are relative rather than absolute. This allows us to analyze all 32 records from test PP4 with the exception of some late data, 21 records from tests PP5, 23 from PP6, 29 from PP7, and 31 from PP8 [*Vesselinov*, 2000]. The total number of pressure records we analyze is thus 136.
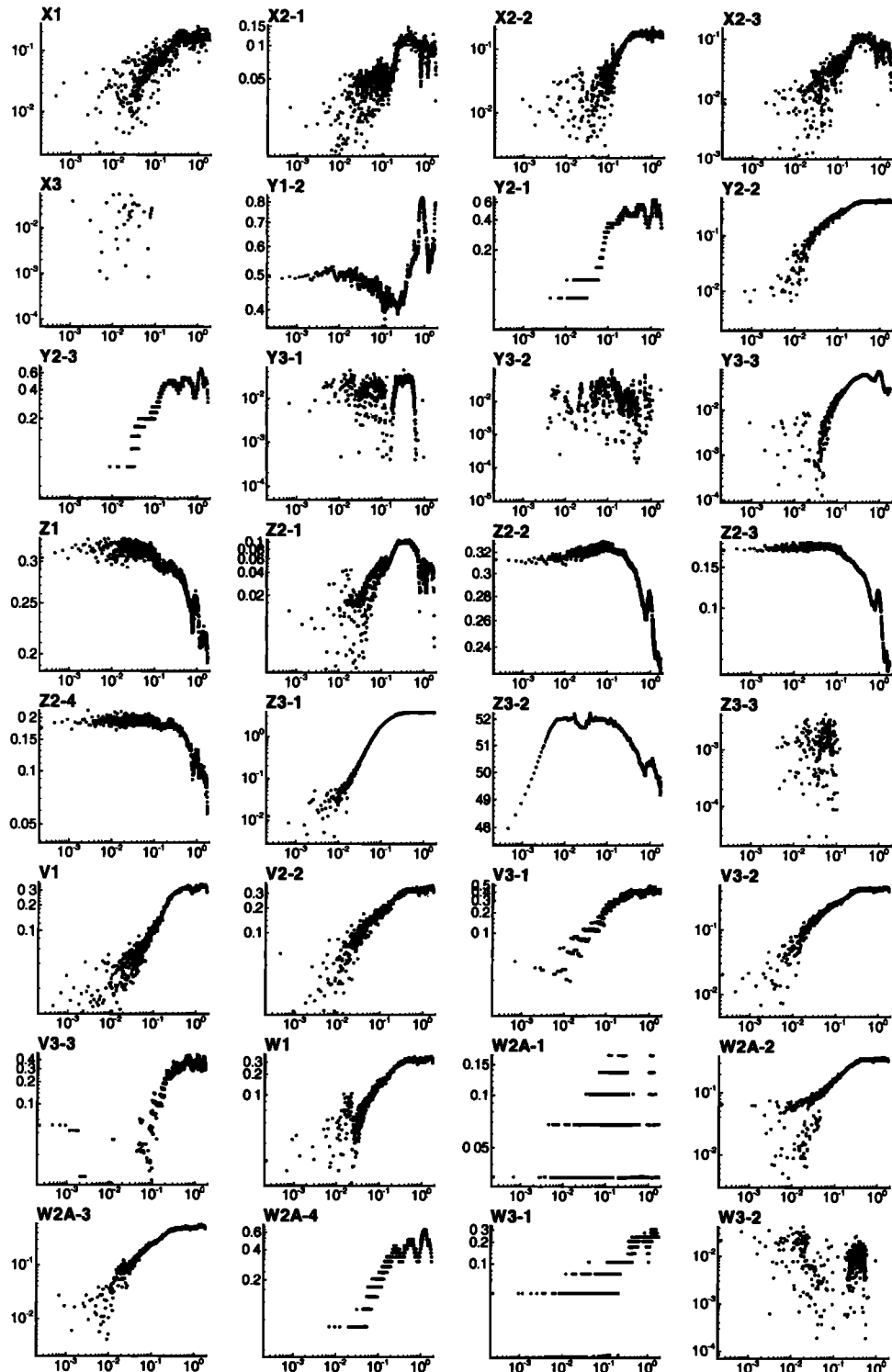
Figure 4. Log-log plots of observed pressure buildup (kPa) versus time (days) during test PP6.

2.3. Qualitative Analysis of Pressure Responses

Since most monitoring intervals respond consistently to air injection during each cross-hole test, it is reasonable to conclude that air-filled fractures at ALRS are pneumatically well connected. The recorded pressure responses suggest that we should be able to model airflow at the site by treating these fractures as a three-dimensional porous continuum.

Though the fracture network at ALRS is sufficiently interconnected to allow modeling it as a continuum, some of the pressure records nevertheless bear witness to the local influence of discrete fractures. In particular, early pressure data in intervals Y3-1, Z1, Z2-1, Z2-2, Z2-3, Z2-4, and Z3-3 during test PP4 (Figure 2) delineate straight lines having slopes close to 1:2, which suggests that the intervals are intersected by
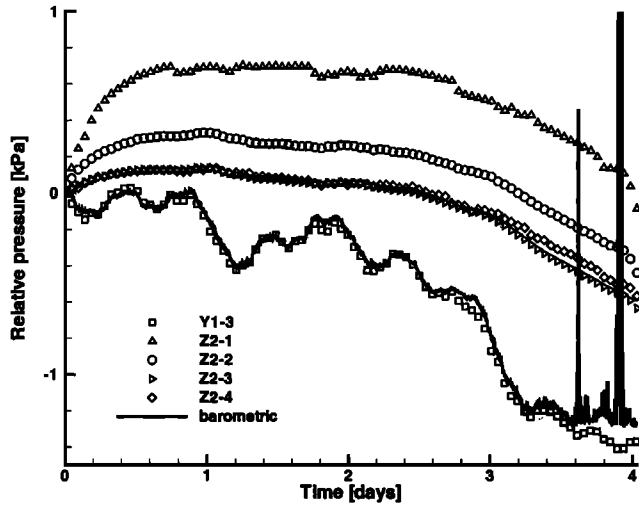
Figure 5. Variations in barometric pressure compared with pressure buildups in selected intervals during test PP4.

discrete planar features of a relatively high permeability [cf. *Raghavan*, 1993]. The fact that pressure in these and neighboring test intervals is influenced by barometric pressure suggests that these features are pneumatically connected to the atmosphere.

Whereas some test intervals intersect high-permeability zones, others are evidently completed in low-permeability segments of the rock. Most strikingly, pressure responses in test interval X3 are consistently much lower than those in other intervals, implying that it must be surrounded by low-permeability rock. It is thus evident that even though the fracture network at the site is sufficiently interconnected to be modeled as a continuum, this continuum is nevertheless strongly heterogeneous. Our conclusion is consistent with an earlier geostatistical analysis of log permeability data from single-hole pneumatic tests at ALRS [*Chen et al.*, 2000; *Vesselinov*, 2000], which has shown that they vary significantly in space and can be modeled as a random fractal field defined over a continuum. We therefore include in our inverse model of the cross-hole tests an option to represent log air permeability, as well as log air-filled porosity, at the site as random fractal fields.

Some of the pressure records in Figures 2, 3, and 4 exhibit behavior that is suggestive of a borehole storage effect at early time. This is true especially for injection intervals and some monitoring intervals located close to them, for example, X2-2, X2-3, Y2-1, Y2-3, Y3-3, and V3-3 during test PP4, as is seen in Figure 2. In these intervals the early pressure data delineate a straight line having a near unit slope, which is typical of borehole storage [*Papadopulos and Cooper*, 1967]. Pressure in the injection interval during test PP6 (Z3-2 in Figure 4) climbs exponentially at early time, which we show later reflects the nonlinear impact of variable air compressibility on borehole storage. We therefore account in our model directly for air storage in (as well as airflow through) packed-off borehole intervals and nonlinearities that arise from the high compressibility of air.

2.4. Air Temperature

Illman et al. [1998] recorded variations in air temperature during each pneumatic test at ground level and within most

monitoring intervals. The records show insignificant variations everywhere except in injection interval Y2-2 during tests PP4 and PP8. Some of the temperature data recorded during test PP4 are depicted in Figure 6; those measured during test PP8 look similar and are therefore not shown. Though the injected air was much warmer than ambient air in the rock, air injection at a high rate caused temperature in the injection interval to decrease. The reason might have been rapid adiabatic expansion of injected compressed air, a two-phase air-vapor phenomenon, or a combination of both. Since the effect is localized and not observed in the surrounding intervals, we model airflow during cross-hole tests at ALRS as an isothermal process.

3. Governing Equations

Considering the above observations regarding pressure and temperature variations during pneumatic cross-hole tests at ALRS, we simulate airflow during these tests as follows. Air forms a single-phase fluid within a three-dimensional porous continuum that is either uniform or heterogeneous. Airflow takes place in a domain Ω with boundary Γ. It is governed by the nonlinear partial differential equation [cf. *Bear*, 1972, p. 200]

$$\nabla \cdot \left(\frac{k\rho}{\mu}\nabla p\right) + \frac{\partial}{\partial z}\left(\frac{kg\rho^2}{\mu}\right) + q_w = \phi\frac{\partial\rho}{\partial t} \quad (1)$$

subject to the following initial and generalized boundary conditions:

$$p = p_0 \quad (2)$$

in Ω at $t = 0$

$$\left(\frac{k\rho}{\mu}\nabla p\right) \cdot \mathbf{n} = v(p_f - p) + q_b \quad (3)$$

along Γ, where k is air permeability $[L^2]$, ρ is air density $[M/L^3]$, μ is air dynamic viscosity $[M/LT]$, p is absolute air pressure $[M/LT^2]$, z is the vertical coordinate $[L]$, g is acceleration due to gravity $[L/T^2; 9.8$ m/s$^2]$, q_w is an internal air source $[M/L^3T]$, ϕ is air-filled porosity [dimensionless], $\mathbf{n}$ is a
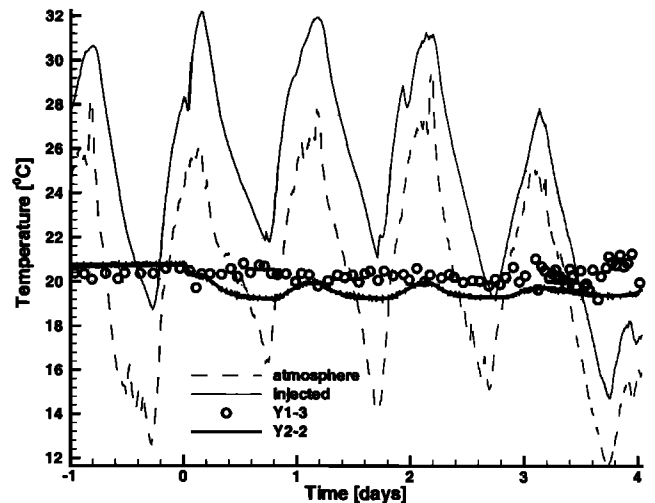

Figure 6. Some air temperature measurements collected during test PP4.

unit outward normal to Γ, v $[T/L]$ is a parameter controlling the type of boundary condition (Neumann or Dirichlet if $v = 0$ or $v \to \infty$, respectively; mixed otherwise), p_f is prescribed air pressure $[M/LT^2]$ on the boundary Γ, and q_b is prescribed air mass flux $[M/L^2 T]$ normal to Γ. The absolute air pressure p [N/m^2] and air density ρ [kg/m^3] are related through the equation of state

$$\rho = pM_m/ZRT, \tag{4}$$

where Z is a dimensionless compressibility factor depending on air pressure and temperature, M_m is molecular mass [kg/mol], T is absolute temperature [K] and R is the universal gas constant [8.314 J/(K mol)]. Within the range of pressures and temperatures registered during pneumatic tests at ALRS, Z remains virtually equal to 1 [Illman et al., 1998].

To account for the storage of air in packed-off borehole intervals, we include in our model a mass balance equation for each interval,

$$Q_{inj} - Q = \partial M/\partial t, \tag{5}$$

where Q_{inj} is the mass rate at which air is injected into the interval (equal to 0 in monitoring intervals), Q is the mass rate at which air flows from the interval into the surrounding rock, and M is the mass of air within the interval. The right-hand side of (5) can be rewritten as

$$\frac{\partial M}{\partial t} = \frac{\partial M}{\partial p_w}\frac{\partial p_w}{\partial t} = V_w \frac{\partial \rho}{\partial p_w}\frac{\partial p_w}{\partial t}, \tag{6}$$

where p_w is air pressure in the borehole interval and V_w $[L^3]$ is its nominal volume. Combining (5) and (6) and introducing the air compressibility $C_a = (1/p)(\partial p/\partial p)$ $[LT^2/M]$ yields

$$Q_{inj} - Q = V_w\rho C_a \frac{\partial p_w}{\partial t}. \tag{7}$$

Since Z is virtually a constant, (4) implies that $C_a \approx 1/p_w$. Disregarding the loss of air pressure within the injection line and considering that for all practical purposes, the temperature T remains constant during the tests, the density of air in the injection line remains equal to that within the borehole interval. Therefore (7) can be rewritten in volumetric form as

$$Q'_{inj} - Q' = V_w C_a \frac{\partial p_w}{\partial t} \approx V_w \frac{1}{p_w}\frac{\partial p_w}{\partial t}, \tag{8}$$

where $Q' = Q/\rho$ $[L^3/T]$. The term on the right-hand side of (8) represents volumetric rate of change in storage within the borehole interval. We note that the rate of borehole storage decreases with an increase in absolute air pressure within the interval. It also decreases as the rate of pressure variation in the interval goes down (i.e., as air pressure in the interval stabilizes).

During the early part of a pneumatic injection test, airflow from the injection interval into the rock is virtually zero, and (8) can be expressed in dimensionless form as

$$\Delta \bar{p}_w = \exp(\bar{t}) - 1, \tag{9}$$

where $\Delta \bar{p}_w = (p_w - p_0)/p_0$ is dimensionless pressure buildup and $\bar{t} = t(Q'_{inj}/V_w)$ is dimensionless time. This yields a near-exponential curve when pressure buildup in the injection interval is plotted versus time on log-log paper. At times corresponding to $\bar{t} \ll 1$, (9) can be further approximated to first-order by

$$\Delta \bar{p} \approx \bar{t}. \tag{10}$$

This delineates a straight line with unit slope when pressure buildup in the injection interval is plotted versus time on log-log paper. Such a straight line is characteristic of borehole storage in cases where fluid compressibility either is, or can be approximated by, a constant.

4. Numerical Approach

We simulate the pneumatic tests by means of a three-dimensional finite element/finite volume heat and mass transfer code, FEHM version 96-05-07 [Zyvoloski et al., 1997]. Our decision to use FEHM was based in part on the ability of this code to simulate nonisothermal two-phase flow of air and water in dual porosity and/or dual permeability continua and to account for discrete fractures should the need to do so arise (it never did). We use FEHM to simulate three-dimensional isothermal gas flow in a single porous continuum, as described by (1)–(4). The storage properties of packed-off borehole intervals are accounted for via (7). Though air viscosity, μ, depends on absolute pressure, FEHM ignores this dependence. This is justified within the ranges of pressure and temperature recorded during pneumatic tests at ALRS [Illman et al., 1998]. In our simulations, μ is set equal to air viscosity at standard conditions ($T = 20°C$ and $p = 101$ kPa), equal to 1.82×10^{-8} Pa s.

Spatial discretization of the governing equations is done on a three-dimensional computational grid of tetrahedral elements. Since we treat the rock as being pneumatically isotropic on the local scale, we use the finite volume (integrated finite difference) option of FEHM, which is computationally more efficient than finite elements. The volume associated with each node is defined using three-dimensional Voronoï diagrams based on Delaunay tessellation [Watson, 1981]. Air permeability k and air-filled porosity ϕ are defined at nodes and are taken to represent average pneumatic parameters over the corresponding control volumes.

Replacing spatial and temporal derivatives in (1) by finite differences and multiplying by the finite volume V_j leads to the following local flow equation for node j at time step s:

$$\sum_{i=1}^{W} \frac{k_{ij}}{\mu}(\rho_i^s + \rho_j^s)\frac{\rho_i^s - \rho_j^s}{\Delta l_{ij}}S_{ij} + \frac{k_j g}{\mu}(\rho_j^s)^2 S_{zj} + q_j V_j$$

$$= \phi_j \frac{\rho_j^s - \rho_j^{s-1}}{\Delta t_s}V_j, \tag{11}$$

where subscripts and superscripts identify node and time step, respectively; W is the number of nodes contiguous with node j; k_{ij} is the upgradient air permeability between nodes i and j; Δl_{ij} and S_{ij} are the distance and effective flow area between nodes i and j, respectively; S_{zj} is the effective area available for gravity flow around node j; and Δt_s is the length of the sth time step. The geometric parameters W, Δl_{ij}, S_{ij}, S_{zj}, and V_j depend on grid properties and are calculated by FEHM. Time stepping is done using a fully implicit backward difference scheme that is unconditionally stable, first-order accurate in time, and tends to work better for nonlinear problems than does the higher-order time-centered scheme. Upon including initial and boundary conditions in (11), while taking into account the equation of state (4), one can write the former for all nodes as a system of nonlinear algebraic equations
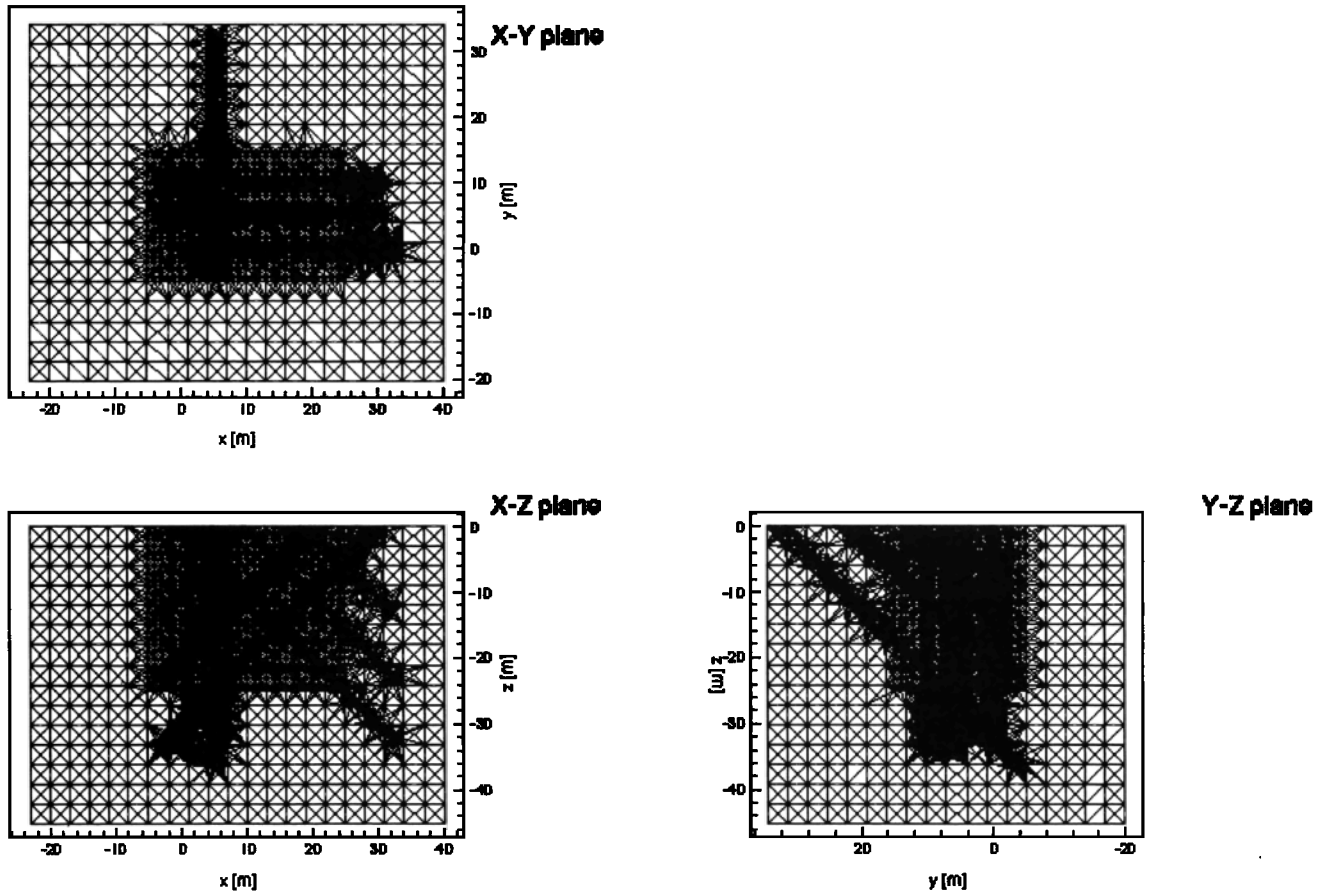
Figure 7. Side views of computational grid for injection into borehole Y2.

$$A(p)p = b(p), \tag{12}$$

where A is a $U \times U$ matrix, b is a U-dimensional matrix, and p is a U-dimensional vector of nodal air pressure values, U being the number of nodes in the grid. The vector b includes information about initial, boundary and source terms. Both A and b depend, in a nonlinear fashion, on the pressure vector p. This system of nonlinear algebraic equations is solved by the Newton-Raphson iterative method. The linear system of equations obtained at each iteration is solved using the Krylov space, nonstationary algorithm GMRES(n), where n is the number of orthogonalizations [*Dongarra et al.*, 1998]. Iterations continue until either the Euclidean ($L2$) norm of pressure variations at each node during an iteration falls below a prescribed tolerance or the allowed number of iterations per time step is exceeded, whichever comes first. FEHM adjusts time step sizes semiautomatically by accounting for the rate at which the Newton-Raphson iterative process converges at each time step.

5. Numerical Simulation of Cross-Hole Tests

Our aim is to simulate selected cross-hole tests and to evaluate the air permeability and air-filled porosity of unsaturated fractured tuff at ALRS by fitting our model to the test data. For this, we consider a three-dimensional computational domain that measures 63 m in the x direction, 54 m in the y direction and 45 m in the z direction, encompassing a rock volume of 153,090 m^3 (Figure 7). The side and bottom boundaries are sufficiently far to have virtually no effect on simulated pneumatic tests, and it is convenient to make them impermeable in our model. The top boundary coincides with the ground surface. As there is no record of absolute barometric pressure fluctuations during the cross-hole tests (only of relative fluctuations), we maintain a constant and uniform barometric pressure at the top boundary. Initial air pressure throughout the flow domain is set equal to that at ground surface. As we simulate only single-phase airflow, the pneumatic properties of the medium remain unchanged throughout the simulations.

Three-dimensional computational grids of tetrahedral elements are generated automatically by means of the code X3D (also known as GeoMesh and LaGriT) [*Trease et al.*, 1996] in a manner that enhances the computational efficiency of FEHM. The grids are visually analyzed and debugged using the code GMV [*Ortega*, 1995]. We use four different grids to simulate cross-hole tests with four different injection intervals in boreholes Y2, X2, Z3, and W3. The number of nodes in these four grids varies from 39,264 to 43,812, and the number of tetrahedral elements varies from 227,961 to 254,310. Each grid consists of a regular portion at the center, with node spacing of 1 m; a surrounding regular portion with node spacing of 3 m; and a much finer and more complex unstructured portion surrounding each borehole. It allows resolving medium heterogeneity in the central part of the domain down to a scale of 1 m^3. This scale of resolution is selected for consistency and
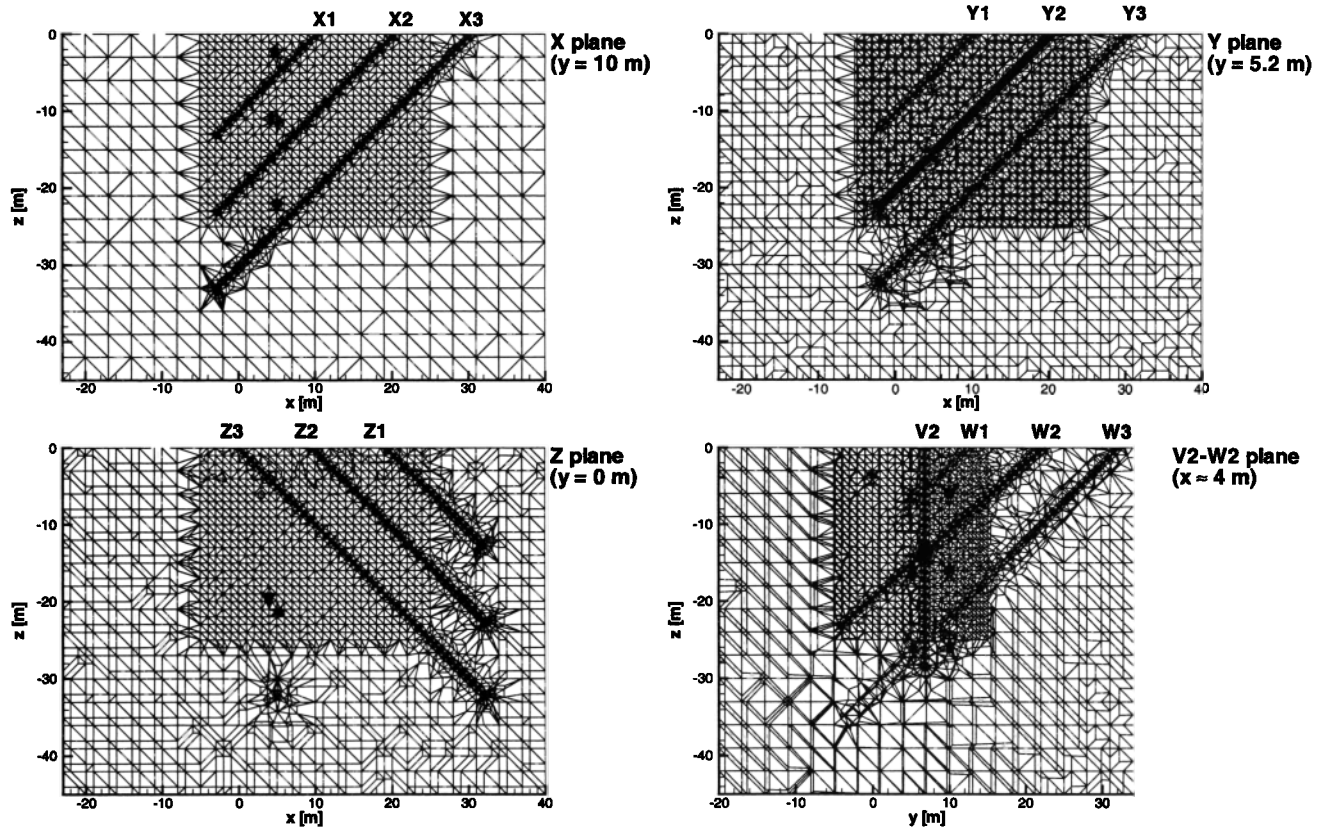
Figure 8. Vertical cross sections through computational grid for injection into borehole Y2.

comparison with single-hole pneumatic injection tests, conducted at the site earlier by *Guzman et al.* [1996]. The single-hole tests yield air permeabilities for the immediate vicinity of each test intervals on a nominal support scale of 1 m³.

We simulate open borehole intervals explicitly by treating them as high-permeability and high-porosity cylinders of finite length and radius. The grid associated with the injection borehole is wider and finer than those associated with other boreholes. This is done so as to allow accurate resolution of relatively high pressure gradients that develop around the injection interval. However, grids surrounding both injection and monitoring boreholes have similar structures. Each is designed so that the sum of computational volumes associated with nodes along the borehole is close to the nominal volume of the borehole. Each borehole grid is additionally refined near the ground surface so as to resolve accurately the flow conditions near this atmospheric boundary. The same is done where boreholes are located close to each other, as happens in the cases of V2 and the W series of boreholes; W2A and W2; W1 and Y1; W3 and Y3. The most complex grid structure is that between boreholes V2 and W2, which intersect each other (Figure 1). There is a gradual transition from fine borehole grids having radial structures and surrounding coarser grids having regular structures.

To illustrate, consider the grid constructed for simulating injection into an interval along borehole Y2. This grid includes 39,264 nodes and 228,035 tetrahedral elements. Figure 7 includes three views of the grid perpendicular to the x-y, x-z, and y-z planes. As the grid in the vicinity of boreholes is relatively fine, the corresponding areas appear dark in the figures. Figure 8 shows four cross-sectional views of the grid along vertical planes that contain selected boreholes. Since the grid is three-dimensional, its intersections with these planes do not necessarily occur along nodal points (i.e., what may appear as nodes in Figure 8 need not be). Figure 9 depicts a 5-m-long segment of the three-dimensional computational grid along injection borehole Y2.

The permeability and porosity of nodes along open borehole intervals are set equal to 3.23×10^{-4} m² and 1.0, respectively. The permeability and porosity of instrumented borehole intervals are set equal to 3.23×10^{-5} m² and 0.5, respectively. At the intersection of boreholes V2 and W2 a lower permeability of 10^{-10} m² is assigned to avoid numerical difficulties. Packers are assigned zero permeability and a nominal porosity of 10^{-5}. In some cases, we selectively "eliminate" boreholes by setting the permeabilities and porosities of nodes along them equal to those of the surrounding rock.

6. Parameterization and Inverse Approach

The forward simulation problem defined by (1)–(4) is well posed and thus guaranteed to yield a unique and stable solution [*Hadamard*, 1932]. The corresponding inverse problem may be ill-posed due to a lack of sufficient information about the state of the system (pressure, flux) and the presence of errors (measurement, interpretation and computation). It can therefore yield nonunique and unstable parameter estimates [*Neuman*, 1973; *Neuman and Yakowitz*, 1979; *Neuman et al.*, 1980; *Neuman*, 1980; *Carrera and Neuman*, 1986a, 1986b].

We simulate pneumatic cross-hole test data in two ways: (1)
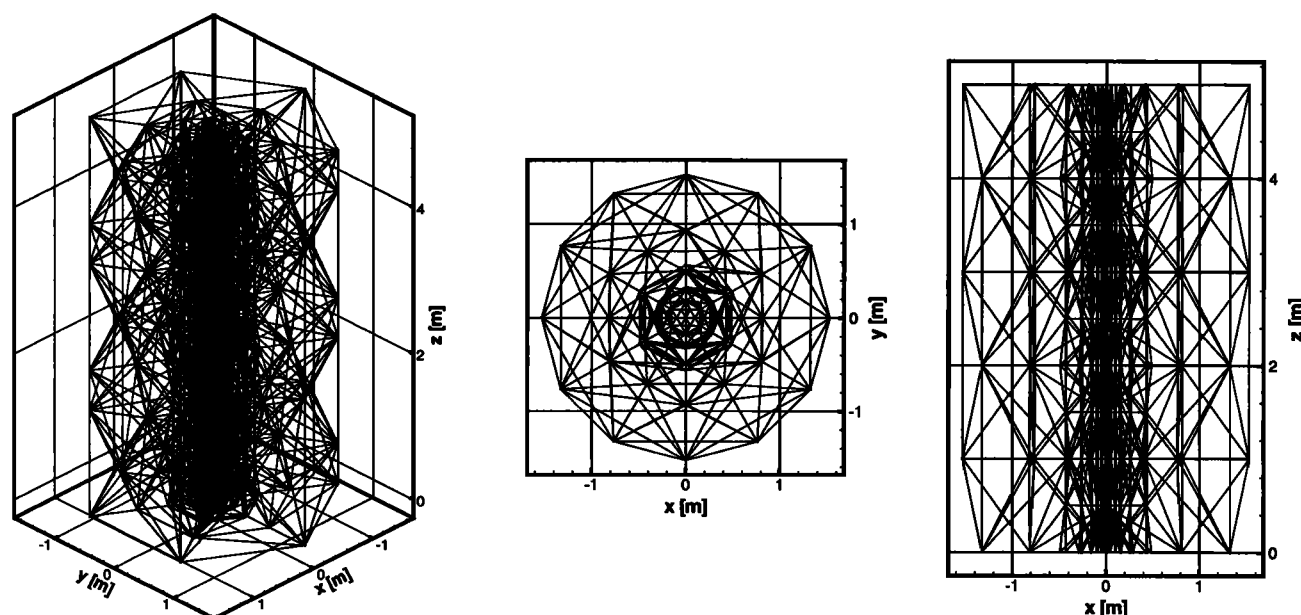
Figure 9. Three-dimensional representation of computational grid along injection borehole.

by treating the rock as being spatially uniform and (2) by treating it as being randomly heterogeneous. In the first case, we assign the same uniform air permeability and air-filled porosity to all nodes in the computational grid. In reality, we estimate these parameters from records of pressure variation with time in individual borehole intervals, one record at a time, by a numerical inverse procedure. This is akin in principle to interpreting each pressure record by the type curve method of *Illman and Neuman* [2001]. It yields a series of equivalent air permeabilities and air-filled porosities for rock volumes having length scales ranging from meters to tens of meters, represented nominally by radius vectors extending from the injection interval to the various monitoring intervals.

In the second case we allow log air permeability $\log_{10} k$ and log air-filled porosity $\log_{10} \phi$ to vary from node to node by interpolating each of them geostatistically (and independently of each other) between values assigned to them at a discrete set of "pilot points." We found through numerical experimentation that placing the majority of between 32 and 72 pilot points along borehole monitoring intervals, and some between these and the injection interval, leads to better results than obtained upon distributing the pilot points more uniformly across the grid. The interpolation is done by "ordinary kriging" [e.g., *Deutsch and Journel*, 1992] over an auxiliary three-dimensional grid of cubic cells measuring 1 m³. In reality, we estimate the parameter values at pilot points from records of pressure variation with time in numerous borehole intervals, as obtained during one or more cross-hole tests, simultaneously by numerical inversion. This amounts to a tomographic interpretation of the pneumatic tests (as proposed in the hydraulic context by *Neuman* [1987]) by means of a geostatistical inverse method that utilizes pilot points (as proposed by *de Marsily* [1978]). It yields a stochastic image of air permeability and air-filled porosity variations across the auxiliary grid at a relatively high spatial resolution of 1 m³.

Our decision to parameterize pneumatic parameters geostatistically is based on the finding [*Chen et al.*, 2000; *Vesselinov*, 2000] that air permeabilities derived from 1-m and 3-m

scale single-hole pneumatic injection tests at ALRS are amenable to geostatistical analysis. This implies that they can be treated as a random field defined at each point in space, supporting *Neuman*'s [1987] opinion that the permeability of fractured rocks can often be viewed as a stochastic continuum. The geostatistical analysis has indicated that log permeabilities from single-hole tests can be associated with a directionally averaged power variogram

$$\gamma(s) = \alpha s^\beta, \tag{13}$$

where s is distance and α and β are positive constants such that $\beta < 2$. This means that the log permeabilities form a random fractal field of the fractional Brownian motion (fBm) type. On the basis of this finding, we associate both log permeability and log porosity in our model with power variograms whose exponents, β, we identify by the inverse method.

Our numerical inverse model identifies simultaneously all unknown values of $\log_{10} k$ and $\log_{10} \phi$ at pilot points by minimizing a suitable error criterion. This criterion consists of the weighted sum of squared deviations between measured and computed air pressures during each test, within all test intervals, at a discrete number of points in time. Prior values of the parameters are used to initiate the process of minimization but not to constrain the final parameter estimates in any way. This insures that the results of previous site characterization studies at ALRS, such as single-hole pneumatic tests and laboratory investigations of rock samples, do not prejudice our inverse analysis of the cross-hole tests. Though we could have relied on the results of single-hole pneumatic tests to better condition our inverse solution, we have purposefully not done so in order to explore the ability of our geostatistical inverse solver to analyze cross-hole pneumatic test data without the help of single-hole test data.

The only constraints we impose on our inverse solution are lower and upper bounds on all parameters, as required by PEST. These bounds are set at -20 and -10 for $\log_{10} k$ and -5 and -0.5 for $\log_{10} \phi$, respectively. We estimate the variogram exponents β either separately or simultaneously with

$\log_{10} k$ and $\log_{10} \phi$ at the pilot points. In the first case, we constrain β to be <1 so as to avoid convergence problems that otherwise arise during the nonlinear iterative process of forward airflow simulation. The multiplier α of the power variogram has no effect on kriging and so is neither needed for, nor can be evaluated by, our inverse model.

Our inverse model utilizes the FEHM code for forward simulation, GSTAT [*Pebesma and Wesseling*, 1998] for kriging, and a parallel version of PEST [*Doherty et al.*, 1994] for parameter estimation. We prefer GSTAT to other geostatistical packages because of its ease of handling inputs and outputs, batch-mode processing capability, option to simulate random fields over unstructured grids, and ability to perform global kriging. The latter feature is especially important to us because it allows GSTAT to krige pilot point data over our structured grid ~200 times faster than we have been able to do with GSLIB [*Deutsch and Journel*, 1992], which relies on local search neighborhoods.

PEST uses a variant of the Levenberg-Marquardt algorithm [*Levenberg*, 1944; *Marquardt*, 1963] to minimize an objective function Φ which represents a weighted sum of squared differences between computed and recorded air pressures in borehole test intervals,

$$\Phi(a) = [p^*(x, t) - p(x, t; a)]^T W[p^*(x, t)$$

$$- p(x, t; a)], \qquad (14)$$

where a is a vector of M model parameters to be optimized, p^* and p are vectors of measured and simulated air pressure values at N match points in space-time, and W is an $N \times N$ diagonal weight matrix. In general, p depend in a nonlinear fashion on a. We implement (14) using unit weights, which renders it equivalent to ordinary least squares. The Levenberg-Marquardt algorithm entails computing a Jacobian (sensitivity) matrix J of simulated pressure derivatives with respect to unknown model parameters ($J_{ij} = \partial p_i / \partial a_j$). To assess parameter uncertainty, we follow the linearized analysis of *Carrera and Neuman* [1986a]. It assumes that (1) the measurement errors are Gaussian and mutually uncorrelated (W is diagonal); (2) the forward model is linear in the close vicinity of the optimal parameter estimates; and (3) the parameter estimation errors are multivariate Gaussian. Then the estimation errors are fully characterized by their (zero) mean and covariance matrix Σ_a, which is given approximately by [*Carrera and Neuman*, 1986a]

$$\Sigma_a = s_p^2 [J^T W J]^{-1}, \qquad (15)$$

where s_p^2 is a scaling factor associated with the covariance matrix $\Sigma_p = s_p^2 W^{-1}$ of pressure measurement errors, assessed a posteriori through $s_p^2 = \Phi(â)/N$, where $â$ is the optimum estimate of the parameter vector a.

A convenient way to express parameter uncertainty is by means of their individual 95% confidence intervals, which are proportional to the respective diagonal terms of Σ_a [*Graybill*, 1976]. A more complete appreciation of parameter uncertainty is obtained through an analysis of the eigenvalues and eigenvectors of Σ_a, which reflect cross correlations among the estimation errors. Since the covariance matrix is positive definite, its eigenvalues are real and its eigenvectors are mutually orthogonal, representing the semiaxes of a hyperellipsoid in M-dimensional space. The components of each eigenvector represent the relative contributions to it by the corresponding parameter estimation errors. Parameters associated with eig-

envectors that have small eigenvalues are less uncertain than those associated with eigenvectors that have large eigenvalues. Parameters associated with a single eigenvector have uncorrelated estimation errors. Parameters associated with multiple eigenvectors have cross-correlated estimation errors.

Carrera and Neuman [1986b] used four identification criteria to differentiate between inverse models having different structures (parameterizations). The criteria support the principle of parsimony in that among alternative models which produce similar results, those with fewer parameters are favored. The four criteria due to *Akaike* [1974], *Akaike* [1977], *Hannan* [1980], and *Kashyap* [1982] are

$$AIC(â) = S(â) + 2M \qquad (16)$$

$$BIC(â) = S(â) + M \log N \qquad (17)$$

$$\phi_M(â) = S(â) + 2M \log (\log N) \qquad (18)$$

$$d_M(â) = S(â) + M \log (N/2\pi) - \log |\Sigma_a|, \qquad (19)$$

respectively, where S is the optimum value of the maximum likelihood function (in our case [*Carrera and Neuman*, 1986a], $S = N + \text{Log}(|W|) + N \log [\Phi(â)/N] + N \log (2\pi)$). We have modified PEST to compute the above statistics and used them to discriminate between inverse models with different numbers of parameters and match points.

PEST approximates the derivatives in the Jacobian matrix J by finite differences. This is easy to implement but computationally intensive, requiring $M + 1$ model runs for forward difference and $2M + 1$ for central difference schemes. However, the runs are mutually independent and so can be conducted efficiently in parallel on multiple processors. We have modified a parallel version of PEST [*Doherty*, 1997] so as to utilize optimally the computational resources of a standard UNIX multiprocessor environment and implemented it on the University of Arizona SGI Origin 2000 cluster of 32 processors. We have further altered PEST to allow efficient restarting of the optimization process, if and when it terminates prematurely, so as to virtually eliminate loss of computational time. We also developed a number of preprocessing and postprocessing codes to allow direct and efficient interfacing between X3D, FEHM, GSTAT, and PEST. We used TECPLOT [*Amtec*, 1997] to represent our results graphically.

7. Influence of Packed-Off Borehole Intervals

Because of the high compressibility of air and marked nonuniformity of the tested rock volume we expect air storage within, and airflow through, packed-off borehole intervals to have a potential effect on air pressure propagation and distribution throughout the rock. There is little information in the literature about such effects. Most notably, *Paillet* [1993] observed that the drilling of an additional observation borehole had impacted drawdowns during a hydraulic test in an aquifer [see also *Pickens et al.*, 1987; *Carrera et al.*, 1996]. Our numerical model is well suited for the analysis of borehole effects because it simulates directly their role in air storage and flow. Indeed, we were able to demonstrate [*Illman et al.*, 1998; *Illman and Vesselinov*, 1998] that such effects may be quite important for the interpretation of cross-hole pneumatic injection tests. A similar finding was reported later by *Huang et al.* [1999].

Figure 10. Estimates of pneumatic properties for test PP4 obtained with and without consideration of borehole effects.

We illustrate the point by applying our inverse model to cross-hole test PP4 considering pressure records from individual borehole monitoring intervals one at a time, while treating the rock as being spatially uniform (the inverse analysis of PP4 is discussed at greater length in paper 2). We simulate this test in two different ways by either including or not including packed-off borehole intervals in our model. Borehole intervals are excluded from the model by assigning to the corresponding nodes material properties equal to those of the surrounding rock. In both cases, pressure in each interval is calculated as the average of computed pressures at all nodes along it. Estimates of $\log_{10} k$ and $\log_{10} \phi$ obtained for each monitoring interval with and without borehole effects are compared in Figure 10. Neglecting the influence of boreholes causes a systematic increase in the estimates of both parameters by a factor of ~1.4. This means that open test intervals enhance the conductive and storage properties of the medium.

To examine this issue in more detail, we conduct two separate forward simulations of the same cross-hole test with and without borehole effects, using nonuniform $\log_{10} k$ and $\log_{10} \phi$ (those estimated by our inverse model in paper 2). Calculated pressures with and without boreholes are compared in Figure 11. It is clear that the presence of packed-off borehole intervals has a considerable impact on pressure evolution within the test intervals. Accounting for boreholes (solid curves) may cause pressure in an interval to develop either faster or slower, and to be either higher or lower, than in the case where boreholes are excluded (dashed curves).
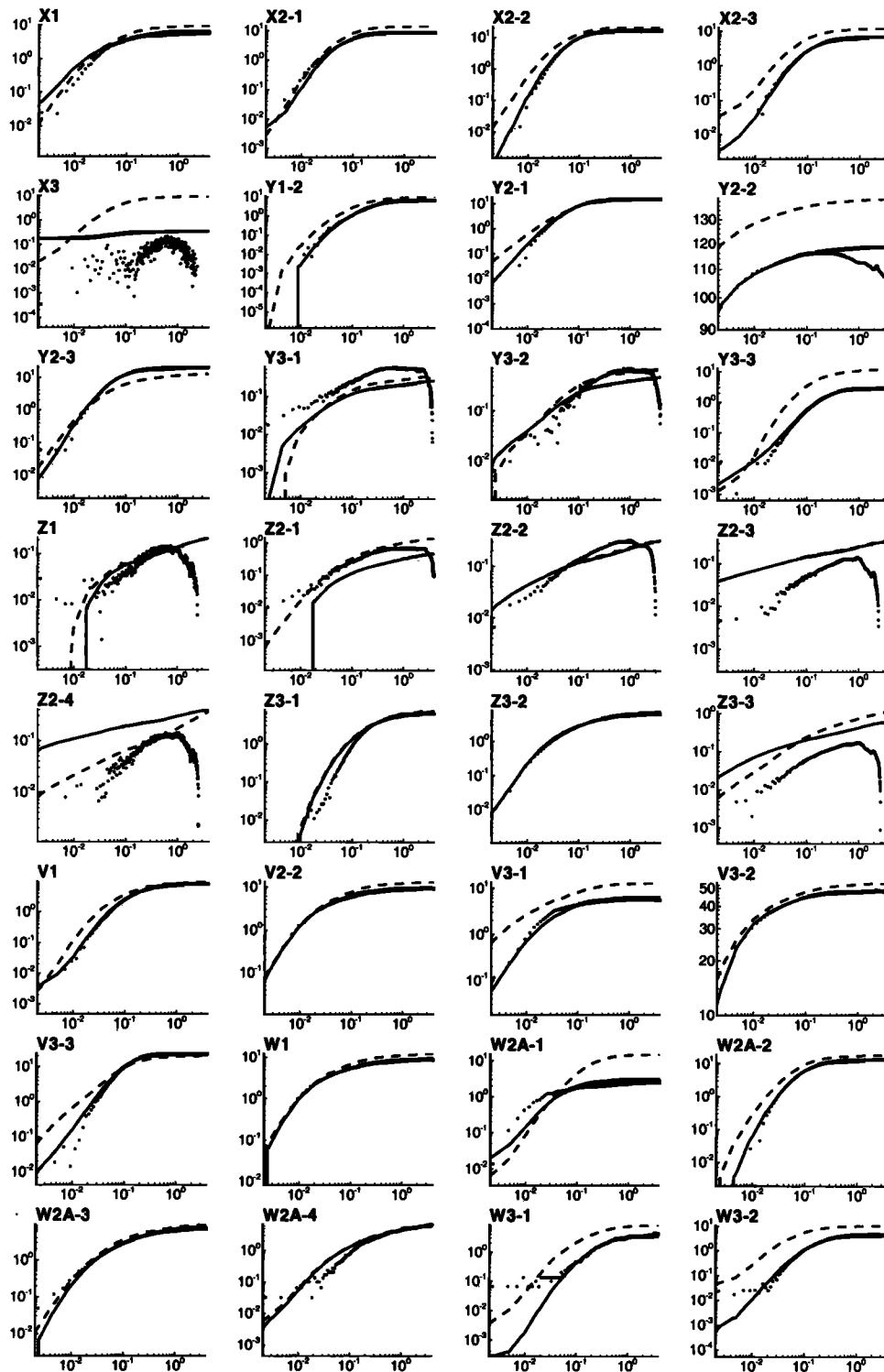
The distributions of computed pressures across two-dimensional vertical sections through the numerical model at the end of test PP4 are shown in Figure 12 for the case where boreholes are included and in Figure 13 for the case where they are excluded. The packer arrangement during this test was depicted earlier in Figure 1. Packers, packed-off borehole intervals and their effects on pressure distribution are clearly evident in Figure 13. Figure 13 also demonstrates that boreholes X2, X3, and Z3 are venting the system. Our imposition of constant pressure at the upper boundary is seen to cause an asymmetric distribution of pressure along vertical sections in both cases. The lateral and bottom no-flow boundaries appear to have a relatively minor effect on pressures in Figures 12 and 13. It is clear that borehole effects must be taken into consideration in the simulation and interpretation of pneumatic tests.

8. Summary

A three-dimensional numerical inverse model has been developed for the interpretation of cross-hole pneumatic tests in unsaturated fractured tuff at the Apache Leap Research Site (ALRS) near Superior, Arizona. The model incorporates the automatic grid generator X3D, the finite volume simulator FEHM, a parallelized version of the parameter estimator PEST, and the geostatistical package GSTAT. It simulates airflow on a three-dimensional grid of structured and unstructured tetrahedral elements, which represents quite accurately the geometry of vertical and inclined boreholes at ALRS. Boreholes are treated in the model as high-permeability and high-porosity cylinders of finite length and radius. Doing so has a considerable effect on airflow, and not doing so may cause a systematic bias in the estimation of pneumatic parameters. Our model treats these parameters either as uniform throughout the rock volume or as random fractal fields. In the first case, the estimated parameters represent equivalent values over rock volumes having length scales ranging from meters to tens of meters, represented nominally by radius vectors extending from the injection interval to the various monitoring intervals. In the second case, they describe the spatial variation of local pneumatic properties throughout the tested rock volume. In our model, this spatial variability is characterized by a power variogram and is estimated geostatistically by kriging on the basis of discrete pilot points. Such estimation entails the simultaneous inversion of pressure records from multiple observation intervals and cross-hole tests. It thus amounts to relatively high-resolution pneumatic tomography, or stochastic imaging, of the rock.

Our three-dimensional inverse modeling approach is novel in its ability to analyze simultaneously transient pressure data from numerous vertical and inclined borehole intervals, during one or more cross-hole tests, within a stochastic framework that yields high-resolution tomographic images of both permeability and porosity for an unsaturated fractured rock. The principle behind our inverse methodology is general and should be applicable to a wide variety of pressure interference tests in both saturated and unsaturated porous and fractured rock environments.

A preliminary inspection of the available cross-hole test data has provided support for our model by suggesting that air-filled fractures at ALRS are pneumatically well connected. Any in-

Figure 11. Log-log plot of simulated pressure buildup (kPa) versus time (days) with (solid curve) and without (dashed curve) borehole effects for test PP4.

fluence of discrete fractures is strictly local, and the fracture network as a whole should be amenable to representation by a three-dimensional porous continuum. This fracture continuum is nevertheless strongly heterogeneous, providing support for our treatment of it as a random field. Some of the cross-hole data reveal evidence of nonlinear behavior and borehole storage effects due to the high compressibility of air, phenomena for which we account explicitly in our model. Temperature remains stable enough to justify modeling airflow during cross-hole tests at ALRS as being isothermal.
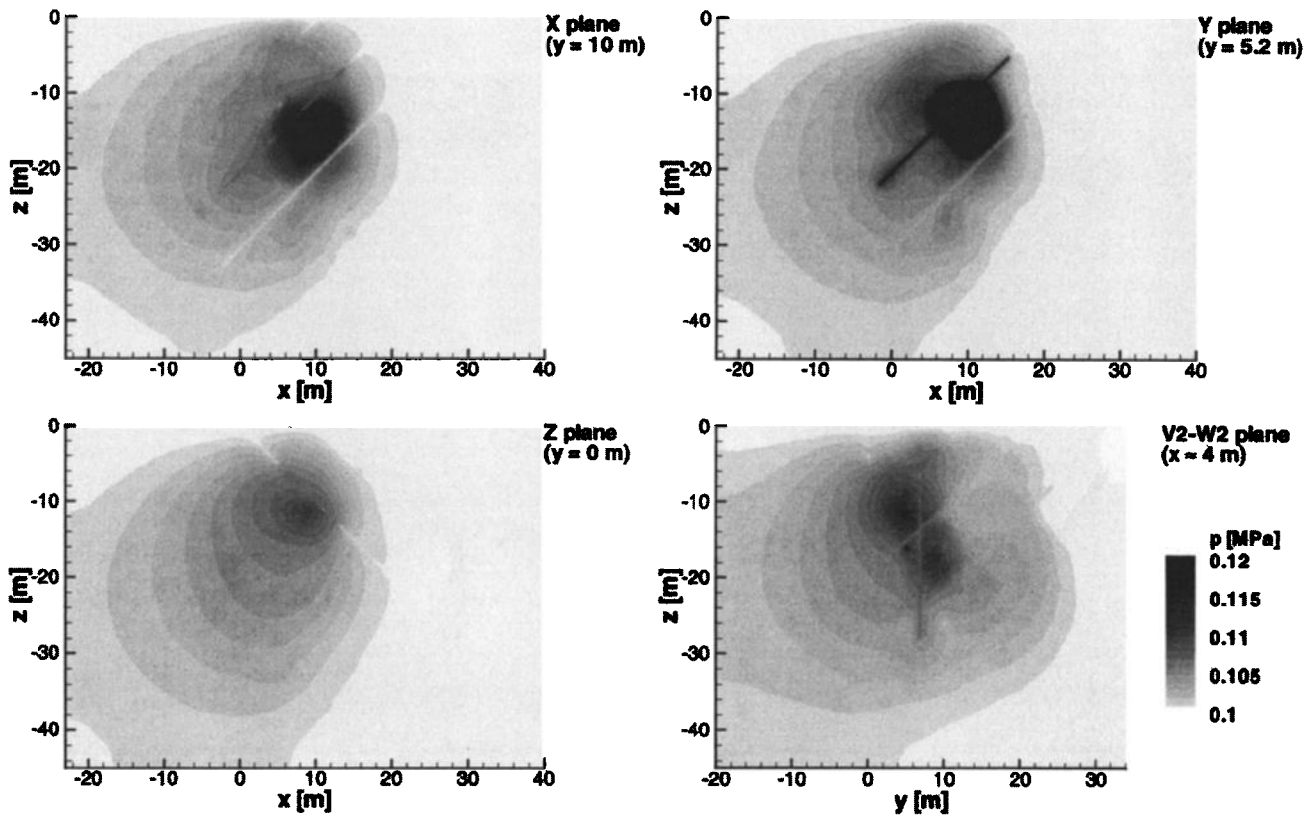
Figure 12. Simulated air pressure [MPa] in computational region at the end of test PP4 with borehole effects.
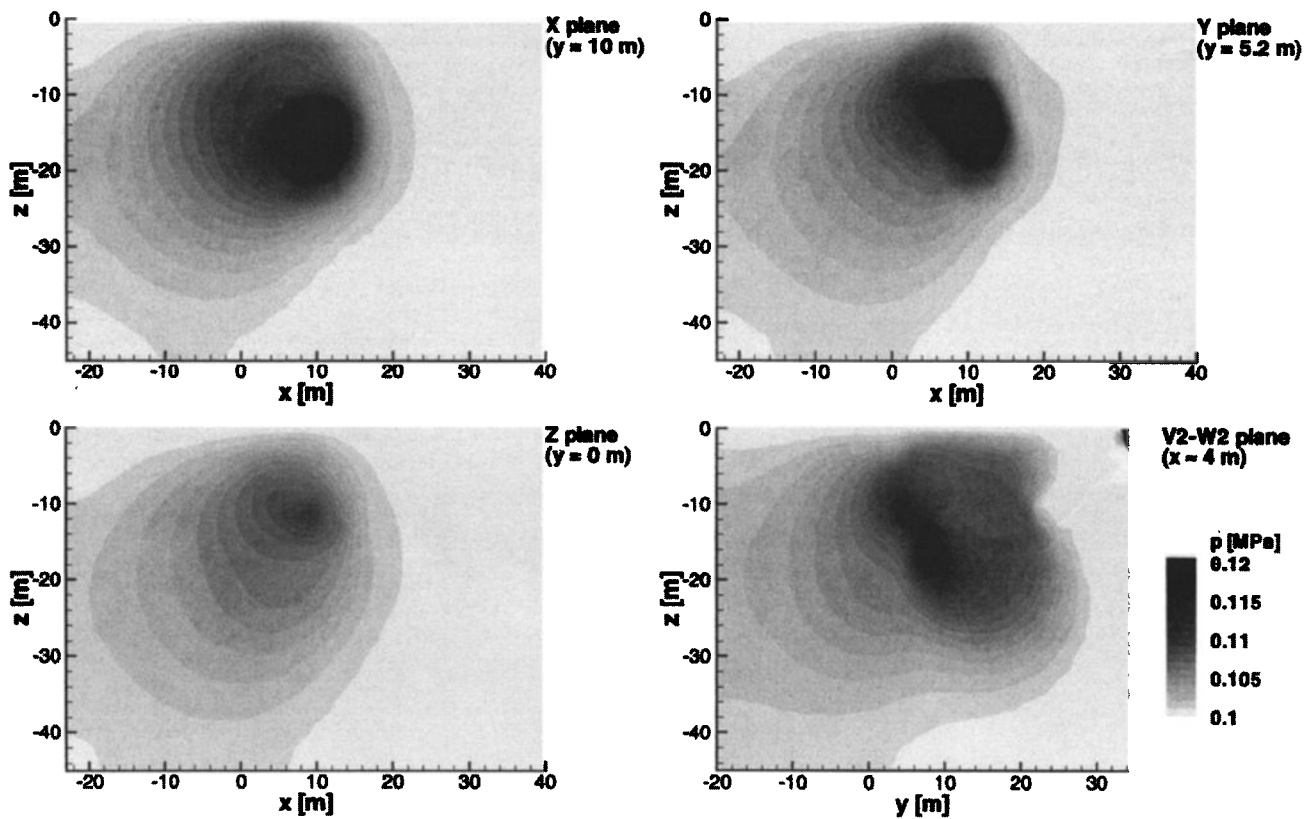

Figure 13. Simulated air pressure [MPa] in computational region at the end of test PP4 without borehole effects.

References

Akaike, H., A new look at statistical model identification, *IEEE Trans. Autom. Control, AC19*, 716–723, 1974.

Akaike, H., On entropy maximization principle, in *Application of Statistics*, edited by P. R. Krishnaiah, pp. 27–41, North-Holland, New York, 1977.

Amtec, Tecplot 7.0 user's guide, Amtec Eng. Inc., Bellevue, Wash., 1997.

Bear, J., *Dynamics of Fluids in Porous Media*, Elsevier Sci., New York, 1972.

Bohling, G. C., Hydraulic tomography in two-dimensional, steady-state groundwater flow, *Eos Trans. AGU, 74*(16), Spring Meet. Suppl., 141, 1993.

Butler, J. J., C. D. McElwee, and G. Bohling, Pumping tests in networks of multilevel sampling wells: Motivation and methodology, *Water Resour. Res., 35*, 3553–3560, 1999.

Carrera, J., and S. P. Neuman, Estimation of aquifer parameters under transient and steady state conditions, 1, Maximum likelihood incorporating prior information, *Water Resour. Res., 22*, 199–210, 1986a.

Carrera, J., and S. P. Neuman, Estimation of aquifer parameters under transient and steady state conditions, 2, Uniqueness, stability, and solution algorithms, *Water Resour. Res., 22*, 211–227, 1986b.

Carrera, J., L. Vives, P. Tune, M. Saaltink, G. Galarza, J. Guimera, and A. Medina, Interpretation of field tests in low permeability fractured media: Recent experiences, in *Parameter Identification and Inverse Problems in Hydrogeology, Geology and Ecology*, edited by J. Gottlieb and P. DuChateau, pp. 53–70, Kluwer Acad., Norwell, Mass., 1996.

Chen, G., W. A. Illman, D. L. Thompson, V. V. Vesselinov, and S. P. Neuman, Geostatistical, type-curve and inverse analyses of pneumatic injection tests in unsaturated fractured tuffs at the Apache Leap Research Site near Superior, Arizona, in *Dynamics of Fluids in Fractured Rocks, Geophys. Monogr. Ser.*, vol. 122, edited by B. Faybishenko, P. A. Witherspoon, and S. M. Benson, pp. 73–98, AGU, Washington, D. C., 2000.

Cook, P., Analysis of interwell hydraulic conductivity in fractured granite, Master's thesis, Univ. of Calif., Berkeley, 1996.

de Marsily, G., De l'Identifcation des systemes en hydrogeologiques, these de docteur es sciences, Univ. Pierre et Marie Curie-Paris VI, Paris, 1978.

Deutsch, C. V., and A. G. Journel, *GSLIB: Geostatistical Software Library and User's Guide*, Oxford Univ. Press, New York, 1992.

Doherty, J., Parallel PEST, Watermark Comput., Brisbane, Australia, 1997.

Doherty, J., L. Brebber, and P. Whyte, *PEST: Model Independent Parameter Estimation*, Watermark Comput., Brisbane, Queensland, Australia, 1994.

Dongarra, J. J., I. S. Duff, D. C. Sorensen, and H. A. V. der Vorst, *Numerical Linear Algebra for High-Performance Computers*, Soc. for Ind. and Appl. Math., Philadelphia, Pa., 1998.

Gottlieb, J., Hydraulishe Tomographie: Indentifikation Raumlich Verteilter Durchlassigkeiten im Underground, Deutsches Patentamt P4236692.5 30.10.1992, Dtsch. Patent Office, Munich, Germany, 1992.

Gottlieb, J., and P. Dietrich, Identification of the permeability distribution in soil by hydraulic tomography, *Inverse Problems, 11*, 353–360, 1995.

Graybill, F. A., *Theory and Application of the Linear Model*, Wadsworth, Belmont, Calif., 1976.

Guzman, A. G., and S. P. Neuman, Field air injection experiments, in *Apache Leap Tuff INTERVAL Experiments*, edited by T. C. Rasmussen et al., *Rep. NUREG/CR-6096*, pp. 52–94, U.S. Nucl. Regul. Comm., Washington, D. C., 1996.

Guzman, A. G., S. P. Neuman, C. F. Lohrstorfer, and R. L. Bassett, Field hydraulic, pneumatic and tracer tests: Phase I, in *Validation Studies for Assessing Unsaturated Flow and Transport Through Frac-*

tured Rock, edited by R. L. Bassett et al., *Rep. NUREG/CR-6203*, U.S. Nucl. Regul. Comm., Washington, D. C., 1994.

Guzman, A. G., A. M. Geddis, M. J. Henrich, C. F. Lohrstorfer, and S. P. Neuman, Summary of air permeability data from single-hole injection test in unsaturated fractured tuff at the Apache Leap Research Site: Results of steady-state test interpretation, *Rep. NUREG/CR-6360*, U.S. Nucl. Regul. Comm., Washington, D. C., 1996.

Hadamard, D. C., *Le Probleme de Cauchy et Les Equations Aux Derivees Partielles Lineaires Hyperboliques*, Hermann, Paris, 1932.

Hannan, E. S., The estimation of the order of an ARMA process, *Ann. Stat., 8*, 1071–1081, 1980.

Hsieh, P. A., and S. P. Neuman, Field determination of the three-dimensional hydraulic conductivity tensor of anisotropic media, 1, Theory, *Water Resour. Res., 21*, 1655–1665, 1985.

Hsieh, P. A., S. P. Neuman, G. K. Stiles, and E. S. Simpson, Field determination of the three-dimensional hydraulic conductivity tensor of anisotropic media, 2, Methodology and application to fractured rocks, *Water Resour. Res., 21*, 1667–1676, 1985.

Huang, K., Y. W. Tsang, and G. S. Bodvarsson, Simultaneous inversion of air injection tests in fractured unsaturated tuff at Yucca mountain, *Water Resour. Res., 35*, 2375–2386, 1999.

Illman, W. A., Single- and cross-hole pneumatic injection tests in unsaturated fractured tuffs at the Apache Leap Research Site near Superior, Arizona, Ph.D. thesis, Univ. of Ariz., Tucson, 1999.

Illman, W. A., and S. P. Neuman, Type-curve interpretation of multirate single-hole pneumatic injection tests in unsaturated fractured rock, *Ground Water, 38*, 899–911, 2000.

Illman, W. A., and S. P. Neuman, Type-curve interpretation of a cross-hole pneumatic injection test in unsaturated fractured tuff, *Water Resour. Res., 37*, 583–604, 2001.

Illman, W. A., and V. V. Vesselinov, Type-curve and numerical inverse interpretation of single-hole transient pneumatic tests in unsaturated fractured tuffs at the Apache Leap Research Site, paper presented at International Symposium in Honor of Shlomo P. Neuman: Recent Advances After 30 Years of Exceptional Contributions to Well Hydraulics, Numerical Modeling and Field Investigations, Univ. of Ariz., Tucson, 1998.

Illman, W. A., D. L. Thompson, V. V. Vesselinov, G. Chen, and S. P. Neuman, Single- and cross-hole pneumatic tests in unsaturated fractured tuffs at the Apache Leap Research Site: Phenomenology, spatial variability, connectivity and scale, *Rep. NUREG/CR-5559*, U.S. Nucl. Regul. Comm., Washington, D. C., 1998.

Karasaki, K., B. Freifeld, A. Cohen, K. Grossenbacher, P. Cook, and D. Vasco, A multidisciplinary fractured rock characterization study at Raymond Field Site, Raymond, CA, *J. Hydrol., 236*, 17–34, 2000.

Kashyap, R. L., Optimal choice of AR and MA parts in auto regressive moving average models, *IEEE Trans. Pattern Anal. Mach. Intell., 4*, 99–104, 1982.

Levenberg, K. A., A method for the solution of certain nonlinear problems in least squares, *Q. Appl. Math., 2*, 164–168, 1944.

Marquardt, D. W., An algorithm for least-squares estimation of nonlinear parameters, *J. Soc. Ind. Appl. Math., 11*, 431–441, 1963.

Martinez-Landa, L., J. Carrera, J. Guimer'a, E. Vazquez-Sune, L. Vives, and P. Meier, Methodology for the hydraulic characterization of a granitic block, in *ModelCARE99 Calibration and Reliability in Groundwater Modelling: Coping with Uncertainty*, edited by F. Staufer et al., pp. 340–345, Int. Assoc. of Hydrol. Sci., Gentbrugge, Belgium, 2000.

Masumoto, K., H. Tosaka, K. Kojima, K. Itoh, and Y. Otsuka, New measuring system and high speed three dimensional inversion method for hydropulse tomography, in *8th International Congress on Rock Mechanics*, edited by T. Fujii, pp. 847–850, A. A. Balkema, Brookfield, Vt., 1995.

Masumoto, K., H. Tosaka, and K. Kojima, Hydraulic characterization of rock mass by hydropulse tomography, *Proc. Int. Geol. Congr., 30th*, 393, 1996.

Masumoto, K., H. Tosaka, and K. Kojima, New algorithm for identifying hydraulic property distribution of rock mass by simultaneous fitting of pressure and its change rate at multipoints in multi-wells, *J. Groundwater Hydrol., 40*, 273–287, 1998.

Neuman, S. P., Calibration of disturbed parameter groundwater flow models viewed as a multiple-objective decision process under uncertainty, *Water Resour. Res., 9*, 1006–1021, 1973.

Neuman, S. P., A statistical approach to the inverse problem of aquifer

hydrology, 3, Improved solution method and added perspective, *Water Resour. Res.*, *16*, 331–346, 1980.

Neuman, S. P., Stochastic continuum representation of fractured rock permeability as an alternative to the REV and fracture network concepts, *Proc. U.S. Symp. Rock Mech.*, *28th*, 533–561, 1987.

Neuman, S. P., and S. Yakowitz, A statistical approach to the inverse problem of aquifer hydrology, 1, Theory, *Water Resour. Res.*, *15*, 845–860, 1979.

Neuman, S. P., G. E. Fogg, and E. A. Jacobson, A statistical approach to the inverse problem of aquifer hydrology, 2, Case study, *Water Resour. Res.*, *16*, 33–58, 1980.

Ortega, F., GMV: General mesh viewer, *Rep. LAUR 95-2986*, Los Alamos Natl. Lab., Los Alamos, N. M., 1995.

Paillet, F. L., Using borehole geophysics and cross-borehole flow testing to define connections between fracture zones in bedrock aquifers, *J. Appl. Geophys.*, *30*, 261–279, 1993.

Papadopulos, I. S., and H. H. Cooper, Drawdown in a well of large diameter, *Water Resour. Res.*, *3*, 241–244, 1967.

Pebesma, E., and C. Wesseling, GSTAT, a program for geostatistical modelling, prediction and simulation, *Comput. Geosci.*, *24*, 17–31, 1998.

Pickens, J. F., G. E. Grisak, J. D. Avis, D. W. Belanger, and M. Thury, Analysis and interpretation of borehole hydraulic tests in deep boreholes: Principles, model development, and applications, *Water Resour. Res.*, *23*, 1341–1375, 1987.

Raghavan, R., *Well Test Analysis*, Prentice-Hall, Old Tappan, N. J., 1993.

Rasmussen, T. C., D. D. Evans, P. J. Sheets, and J. H. Blanford, Unsaturated fracture rock characterization methods and data sets at the Apache Leap Tuff Site, *Rep. NUREG/CR-5596*, U.S. Nucl. Regul. Comm., Washington, D. C., 1990.

Sauer, R., R. Greswell, A. Herbert, R. Mackey, and J. Tellam, Model calibration from pump testing of the 3D flow around a test well site, penetrating the Triassic sandstone aquifer, Birmingham, U.K., paper presented at International Conference on Calibration and Reliability in Groundwater Modeling Coping With Uncertainty, Int. Assoc. of Hydrol. Sci., Zürich, Switzerland, Sept. 20–23, 1999.

Tosaka, H., K. Masumoto, and K. Kojima, Hydropulse tomography for identifying 3-D permeability distribution, paper presented at 4th Annual International Conference on High Level Radioactive Waste Management, Am. Soc. of Civ. Eng., Reston, Va., 1993.

Trease, H. E., D. George, C. W. Gable, J. Fowler, A. Kuprat, and A. Khamyaseh, The X3D grid generation system, in *5th International Conference on Numerical Grid Generation in Computational Fluid Dynamics and Related Fields*, edited by B. K. Soni et al., pp. 239–244, Eng. Res. Cent., Miss. State Univ. Press, Mississippi State, 1996.

Vesselinov, V. V., Numerical inverse interpretation of pneumatic tests in unsaturated fractured tuffs at the Apache Leap Research Site, Ph.D. dissertation, Univ. of Ariz., Tucson, 2000.

Vesselinov, V. V., S. P. Neuman, and W. A. Illman, Three-dimensional numerical inversion of pneumatic cross-hole tests in unsaturated fractured tuff, 2, Equivalent parameters, high-resolution stochastic imaging and scale effects, *Water Resour. Res.*, this issue.

Watson, D., Computing the *n*-dimensional Delaunay tessellation with application to Voronoï polytopes, *Comput. J.*, *24*, 167–172, 1981.

Yeh, T.-C. J., and S. Liu, Hydraulic tomography: Development of a new aquifer test method, *Water Resour. Res.*, *36*, 2095–2105, 2000.

Zyvoloski, G. A., B. A. Robinson, Z. V. Dash, and L. L. Trease, Summary of the models and methods for the FEHM application: A finite-element heat- and mass-transfer code, *Rep. LA-13307-MS*, Los Alamos Natl. Lab., Los Alamos, N. M., 1997.

W. A. Illman, Department of Geosciences, University of Iowa, 121 Trowbridge Hall, Iowa City, IA 52242, USA. (walter-illman@uiwa.edu)

S. P. Neuman, Department of Hydrology and Water Resources, University of Arizona, Bldg. 11, P.O. Box 210011, Tucson, AZ 85721-0011, USA. (neuman@hwr.arizona.edu)

V. V. Vesselinov, Hydrology, Geochemistry, and Geology Group, Los Alamos National Laboratory, EES-6, MS T003, Los Alamos, NM 87545, USA. (vvv@lanl.gov)